Hindawi
Advances in Civil Engineering
Volume 2020, Article ID 4212049, 11 pages
https://doi.org/10.1155/2020/4212049

Research Article

Bearing Capacity Studies on Square Steel Tube Confined Steel Reinforced Concrete Column under Eccentric Load

Tongfeng Zhao

Department of Road and Bridge, Liaoning Provincial College of Communications, Shenyang, China

Correspondence should be addressed to Tongfeng Zhao; ztfgty@sohu.com

Received 14 February 2019; Revised 23 April 2019; Accepted 2 May 2019; Published 15 April 2020

Academic Editor: Libo Yan

In the present study, an experimental research was conducted on square steel tube confined steel reinforced concrete column under eccentric load. The major parameters of the specimens included slenderness ratio, eccentricity ratio, and structural steel reinforced ratio. According to the tested results, the eccentricity ratio, from 0 to 0.55, significantly affects the structural bearing capacity. The slenderness ratio, from 3 to 8, and steel reinforced ratio, from 0.3 to 0.41, slightly affect the capacity. Furthermore, a numerical analysis program was developed, and the calculated results are well consistent with the experimental results. Also, the theoretical formula for eccentrically loaded columns was proposed based on numerical results.

1. Introduction

The composite steel-concrete columns have been used in high-rise and long-span buildings extensively. With the booming of urban construction, columns should bear higher load owing to the height and span extension of buildings. They should exhibit the characteristics, e.g., high strength, small cross section, high ductility, and convenience of construction. Also, they must be economical and practical to fit the safety and utilization of buildings.

There are now two traditional types of composite columns, namely, the steel tube columns filled with concrete and steel reinforced concrete.

For the steel tube filled with concrete, effective lateral confinement has been provided to concrete by steel tube to improve the overall ductility and strength. In the meantime, steel tube can serve as a formwork, thereby accelerating the construction process. The concrete around the steel tube can defer the local buckling of the steel tube. However, steel tube filled with concrete has a lower fire resistance than concrete-encased steel columns. On the other hand, the existence of steel in reinforced concrete can improve the shear resistance and antiseismic performance of the column. The encasement of concrete makes the steel more effective against both local and overall buckling, which enhances the stiffness of the specimen. Also, the concrete can provide protection for the steel against chemical corrosion and fire. The major disadvantage of steel reinforced concrete is that reinforced cage and formwork should be set up, thereby making the construction process complicated and construction speed slow.

Based on the studies of steel tube filled with concrete and steel reinforced concrete, a novel composite column of steel tube confined steel reinforced concrete (STSRC) has been studied in recent years [1–5]. The composite column is formed by inserting structural steel reinforced into the steel tube. Subsequently, the whole case is filled with concrete. It maintains the advantages of both steel tubes confined concrete and steel reinforced concrete, e.g., high capacity, high strength, good fire resistance, smaller section, and good shear resistance as well as antiseismic property.

According to the sectional shape of the steel tube, STSRC can be separated into cylinder, square, and rectangular types. I-shape and cross shape are divided according to reinforced steel (Figure 1).

The major confinement of square steel tube occurs at the corners and core position. Thus, its effect of confinement

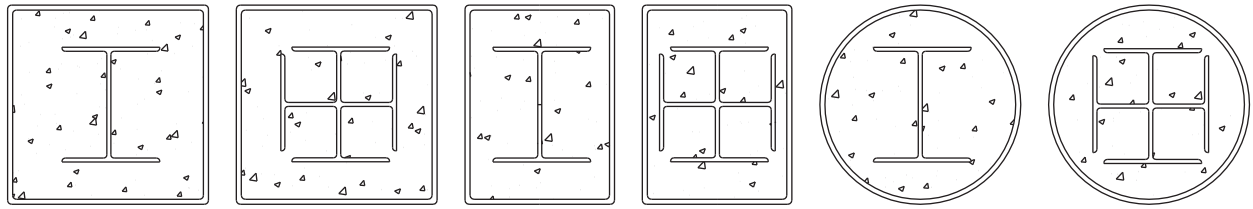

Figure 1: The section types of STSRC.

and bearing capacity is lower than that of the circular steel tube. But it is found that confinement to core concrete provided by square tube can improve the ductility of the specimen. In this way, square steel tube-confined concrete embodies almost all the advantages of circular steel tube-confined concrete to a great extent. Furthermore, square tube-confined concrete has the advantages of large stiffness of bending, simplicity of node domain, convenience of connection, and easiness for indoor layout. It can be confirmed that economic and social benefits are achieved in practical engineering.

Patel et al. studied the verification of a multiscale numerical model described in a companion paper and an extensive parametric study on the performance of high-strength thin-walled rectangular CFST slender beam-columns under biaxial loads. Comparisons of computer solutions with existing experimental results were made to examine the accuracy of the multiscale numerical model developed [6]. Zhao et al. experimentally studied the effect of axial compressive load and eccentric load. According to the results, the propagation of cracks in core concrete can be put off or avoided by the inserted structural steel, so the ultimate bearing capacity and ductility of the composite column are effectively improved [1, 2]. Jung and Mahmoud developed a new direct tension test setup for cylindrical specimens similar to those used in the compression test. The experimental and numerical results of the cracking location showed that gravity effect on fresh concrete during setting time might affect the distribution of concrete cracking strength along the height of the structural elements [7]. Zhao and Wang studied the calculation on compression-bending, axial loading, and pure bending of square tube confined steel reinforced high-strength concrete. Formula for compression-bending was proposed based on the test results [3–5]. Han et al. carried out a series of tests on concrete-filled SHS (square hollow section) stub columns, columns, and beam-columns. A unified theory is described where a confinement factor is introduced to describe the composite action between the steel tube and filled concrete. Simplified models are derived for section capacities and modulus in different stages of the composite sections [8, 9]. Mossahebi et al. carried out an investigation in an effort to comprehend the behavior of a bridge girder consisting of a steel tube confined reinforced concrete. Results of this investigation demonstrated the potential for using a concrete-filled tube as a bridge girder [10]. In addition, there are a large number of research studies on the behavior of steel tube-confined concrete columns under eccentric compression, and also numerical modeling program was developed to study different characteristics of columns [11–19].

Though scholars carry out some research on STSRC, Zhao and Wang [3] deduced the formulas for calculating eccentric bearing capacity using superposition method, but it is too complicated to use in practice. Zhao et al. [1] only studied the formulas for circular columns under eccentric loading. It indicates further research on STSRC is needed, such as more experiments to study its properties and simplified calculation. In this study, an experimental research was conducted on square steel tube column confined steel reinforced concrete subjected to eccentric load. Furthermore, numerical analysis program was developed. Also, theoretical formula for eccentrically loaded columns was proposed by analyzing primary parameters and numerical results. Thus, the safety requirements for engineering structure under eccentricity can be met.

2. Test Method

2.1. Survey of Test. A total of nine specimens were constructed and tested under eccentric load. A summary of the specimens is presented in Table 1. The width of the stub specimens (B) is 200 mm, and the thickness (t) is 5 mm, respectively. Tension tests were carried out to determine the material properties of the steel tubes and steel section. The cross sections of steel tube are cold-formed. The tensile coupons are from the sidewalls of the steel tubes. The yield strength (f_{sy}) and ultimate tensile strength (f_{sy}) of the steel tube are 350 MPa and 425 MPa, respectively. The tensile coupons are from the flanges of the steel section. The yield strength (f_{sy}) and ultimate tensile strength (f_{su}) of the steel section are listed in Table 1. The compressive cube strength (λ) of concrete is 48.4 MPa. Cross section of the steel section is I-shape. The major parameters of the specimens included slenderness ratio λ ($\lambda = L/B$), from 3 to 8, eccentricity ratio e/r (e is initial eccentricity $r = B/2$), from 0 to 0.55, and steel section index ρ ($\rho = A_s f_{sy}/A_c f_{ck}$, where A_s and A_c are the area of concrete and steel cross section, respectively), from 0.3 to 0.41. Confinement index θ ($\theta = A_t f_{ty}/A_c f_{ck}$, where A_t is the area of steel tube) is 0.87.

In this table, 10I, 12I, and 14I denote the height of steel sections which are 100 mm, 126 mm, and 140 mm, respectively. Detailed information is available in [20]. N_{ue} is the tested bearing capacity; N_{us} is the numerical bearing capacity; N_{uc} is the calculated bearing capacity of equation (3) in Section 3.

Table 1: Tested parameters and results.

Specimen no.	L (mm)	A_s mm^2	e/r	f_{sy} (MPa)			N_{ue} (kN)	N_{us} (kN)	 (kN)		N_{ue}/N_{us}
PY10I-0-3	600	1433	0	355	420	0.3	3740	—	—	—	—
PY10I-25-3	600	1433	0.25	355	420	0.3	3216	2888	2870	1.114	1.121
PY10I-40-3	600	1433	0.4	355	420	0.3	2693	2503	2490	1.076	1.082
PY10I-55-3	600	1433	0.55	355	420	0.3	2365	2209	2205	1.071	1.073
PY10I-40-4	800	1433	0.4	355	420	0.3	2670	2468	2457	1.082	1.087
PY10I-40-6	1200	1433	0.4	355	420	0.3	2608	2375	2370	1.103	1.110
PY10I-40-8	1600	1433	0.4	355	420	0.3	2512	2297	2268	1.094	1.108
PY12I-40-3	600	1810	0.4	320	425	0.35	2725	2555	2500	1.067	1.090
PY14I-40-3	600	2150	0.4	420	545	0.41	2833	2686	2651	1.055	1.069

The manufacturing process of the specimens that experienced several phases is as follows.

First, the steel tube and steel section were accurately cut to size, and then the end of the steel section was welded to an end plate (thickness is 25 mm), focusing on keeping the steel section perpendicular to the end plate. Subsequently, strain gauges were glued to the estimated area. Moisture-proof processing was performed using epoxy resin. Steel tube was welded carefully to the end plate to assure that the steel reinforced can lie in the center of the steel tube.

Second, concrete was poured into the tube gradually, and vibrating stick was used to compact the concrete. A very small amount of longitudinal shrinkage occurred at the top of the specimens during the curing process. Thus, before the test, the top surface of the specimens was covered with cement to ensure that steel tube, concrete, and steel reinforced could bear the load simultaneously.

Finally, ribbed slab was welded to solidify the ends of the specimen (Figure 2) to avoid its breaking prior to other components.

2.2. Test Setup and Procedures. All the specimens were tested using a 5000 kN capacity universal testing machine. Eccentric load was imposed on the specimens through the groove hinge and the spherical hinge.

Figure 2 shows that strain gauges are distributed in the midheight of the specimen. Eight longitudinal strain gauges were placed at the external surface of the steel tube, and four transverse strain gauges were placed at the axial of the steel tube. Another three longitudinal strain gauges were placed at the flanges and webs of steel sections. Three displacement transducers were placed at the midheight and the quarter-height of the specimen along the bending direction. A displacement transducer was used to monitor the axial deformation. All the data were collected through UCAM-70A automatically.

Stepped load approach was used in the test. A load of one-tenth of the computed ultimate bearing capacity was applied when the specimen was in elastic range; a load of one-twentieth of the computed ultimate bearing capacity was applied when the load reached 60% of the computed ultimate bearing capacity. Finally, the load was applied continuously until it reached the computed ultimate bearing capacity. The test was completed when the applied load was less than 80% of the ultimate bearing capacity.

2.3. Results and Discussions. There were no significant changes before the eccentric load surpassed 60% of the ultimate bearing capacity. Many diagonal tiny wrinkles were observed from the surface of the steel tube after the axial load surpassed 60% of the ultimate bearing capacity. Sounding occurred when load was close to the ultimate bearing capacity due to cracking of the concrete. Local buckling can be observed in the midheight and quarter-height regions along the length of the specimen. Iron scraps dropped from the surface of the steel tube close to the local buckling regions. Figure 3 gives a general view of the specimens after the test.

The load (N) versus extreme fiber compressive and tensile strains (ε) are shown in Figure 4 for steel tube and steel section, respectively. When the load was small, the strain at midheight is approximately proportional to the applied load. When the load reaches about 60–80% of the maximum load, the lateral strain at midheight started to increase significantly, due to the steel section is located near the center of the whole section. When the load reaches about 70–90% of the maximum load, the lateral strain at midheight started to increase significantly.

It was found that, in general, the measured strain of typical specimen (PY10I-40-3) conforms to the assumption of plane (Figure 5), and the measured deflection curves are in the shape of a half-sine wave (Figure 6).

Curves of Poisson ratio (ν) versus N/N_u are shown in Figure 7. In general, when $N/N_u < 0.7$, the Poisson ratio of concrete is less the Poisson ratio of steel tube (0.3). Above this load level, the steel tube walls at transverse strain gauges begin to confine the concrete ($\nu > 0.3$).

Curves of N versus midheight deformation (u_m) are plotted according to the tested data (Figure 8). It can be stratified into elastic, elastic-plastic, and plastic phases. Deflection of slender specimens was insignificant before the load reached 0.6-0.7 N_u with a linear relationship of N and u_m. Above this load level, the deformation of midheight increased gradually. The deflection increased rapidly when the load approached the N_u. This is considered the elastic-plastic phase. The increased lateral displacement caused the effect of the secondary moment to grow stronger. The load began to drop and the curve of N versus u_m fell into descending phase. This is considered the plastic phase.

The influences of primary parameters on ultimate bearing capacity (Figure 9) show that the bearing capacity decreased when the eccentricity increased. As the eccentricity changes from 0 to 55, the bearing capacity drops to

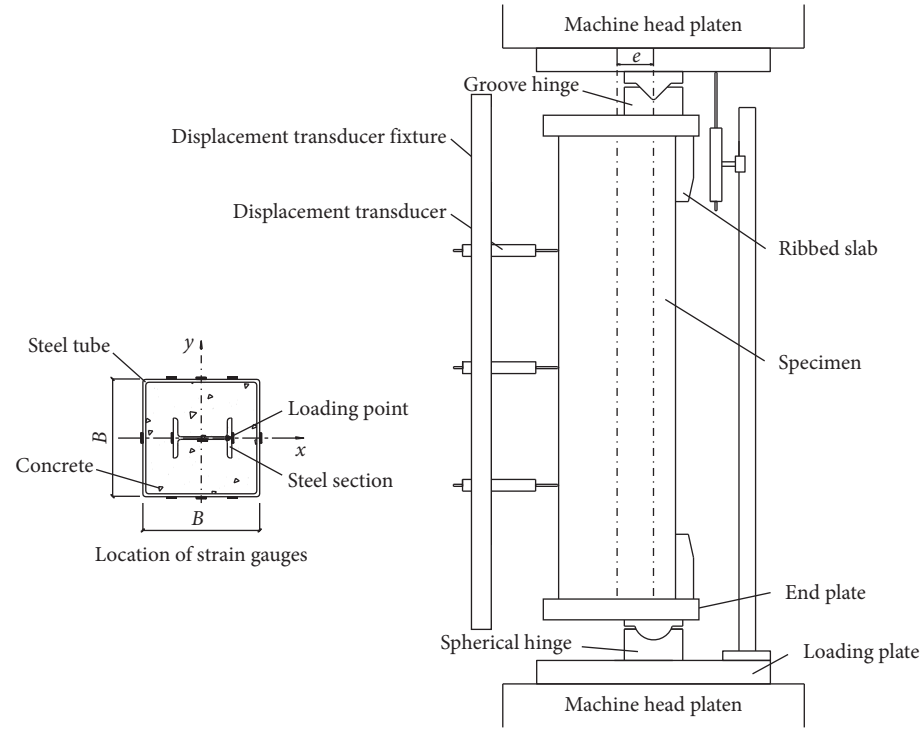

Figure 2: The layout of test.

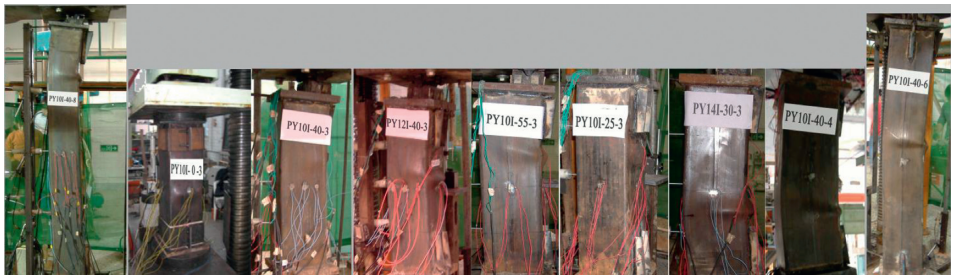

Figure 3: The broken specimens under eccentric load.

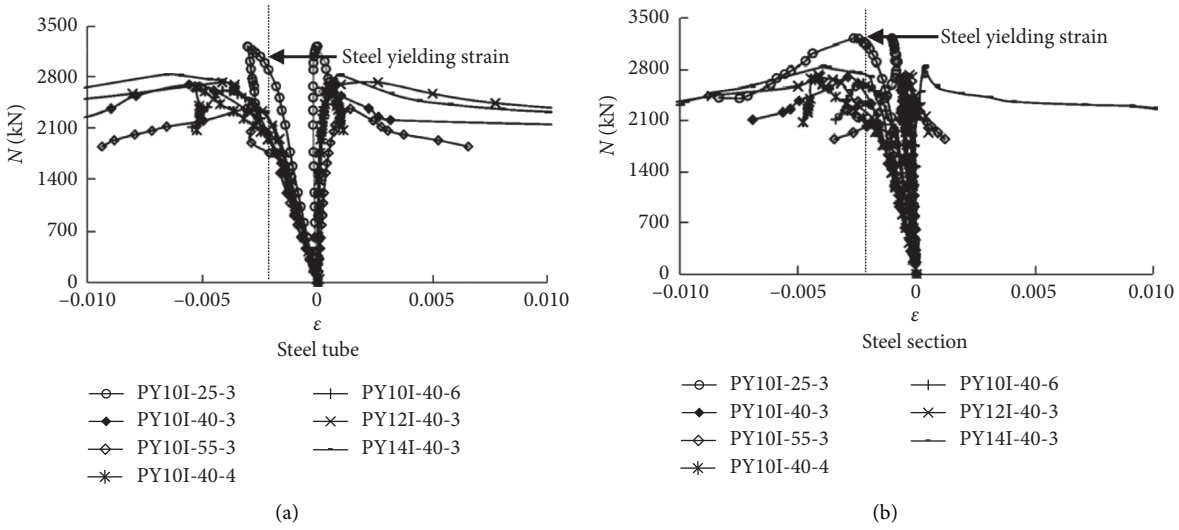

Figure 4: Curves of load-longitudinal strain on (a) steel tube and (b) steel section.

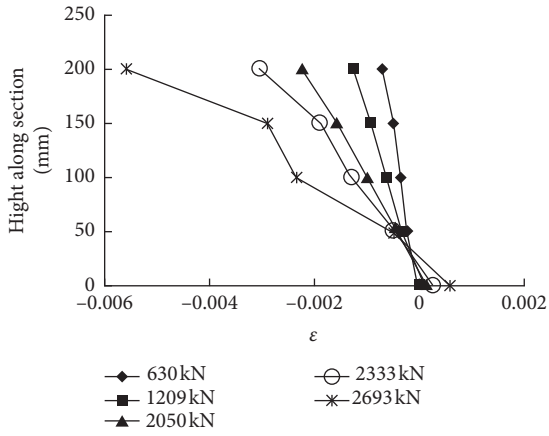

Figure 5: Distribution of longitudinal strain at midsection.

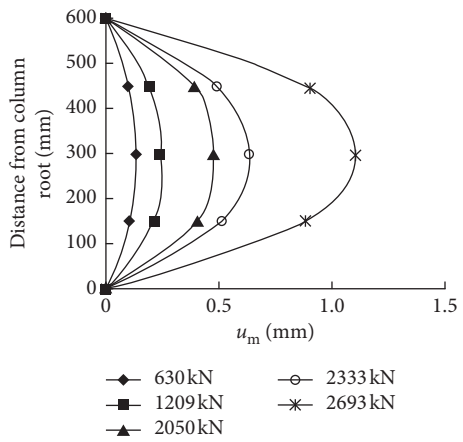

Figure 6: Distribution of deflection along length.

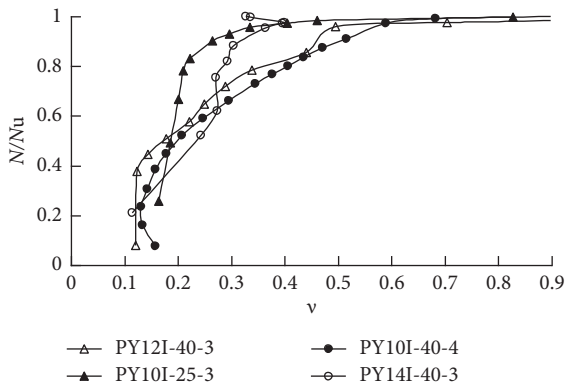

Figure 7: Curves of $N/N_u - \nu$.

40%. As the slenderness ratio changes from 3 to 6, the bearing capacity drops to only 7%. It is shown that a slenderness ratio has a negligible effect on the bearing capacity in tested parameters. This is because the STSRC has high bending stiffness. As steel reinforced changes from 10I to 14I, the steel reinforced ratio increased from 0.3 to 0.41 and bearing capacity increased to only 5%. It also shows that the eccentricity ratio has a significant influence on axial deformation (Δ). Slenderness ratio and steel section ratio have little influence on axial deformation.

3. Theoretical Analysis

3.1. Basic Assumption and Constitutive Model. (1) The strain distribution at midheight conforms to plane cross section assumption. (2) There existed no interfacial slip between the steel and the concrete. (3) The effect of shear on the deformation of the specimen was neglected. (4) Internal and external forces were at equilibrium at midheight only. (5) Hinged connection existed at the ends of the specimen with deflection curve conforming to half-sinusoid.

The constitutive laws of steel and confined concrete were referenced from the study of Zhao and Wang [3].

3.2. Principle and Procedure of Calculation. The cross section of steel tube, concrete, and steel reinforced were stratified into many strips with homogeneously distributed stress. Assume that the strain at the center of cross section is ε_c, the stress of concrete (σ_{ci}), steel reinforced section (σ_{si}), and steel tube (σ_{ti}) can be calculated based on the plane cross section assumption and the stress-strain relationship. Two iterative equations were given for force and moment, respectively:

$$N = \sum_{i=1}^{n} \sigma_{ci} \Delta A_{ci} + \sum_{i=1}^{m} \sigma_{si} \Delta A_{si} + \sum_{i=1}^{n} \sigma_{ti} \Delta A_{ti}, \quad (1)$$

$$M = \sum_{i=1}^{n} \sigma_{ci} \Delta A_{ci} y_{ci} + \sum_{i=1}^{m} \sigma_{si} \Delta A_{si} y_{si} + \sum_{i=1}^{n} \sigma_{ti} \Delta A_{ti} y_{ti}, \quad (2)$$

where n is the number of strips of concrete and steel tube, m is the number of strips of steel reinforced; y_{ci},y_{si}, and y_{ti} refer to the distance from the center of concrete strip, steel reinforced, and steel tube to the center of whole cross section, respectively; ΔA_{ci}, ΔA_{si}, and ΔA_{ti} are the areas of concrete strip, steel reinforced, and steel tube, respectively.

Figure 10 presents the algorithm for the whole computational procedure. First, the stepped deformation Δu_m is applied to specimen, and then curvature ϕ is obtained based on the 5$^{\text{th}}$ assumption. Internal force N_{in} and moment M_{in} are calculated by equation (1) and equation (2). Print the results when differences between internal force and external force are less than error D. Once bearing capacity drops to 80% of the ultimate bearing capacity or when the tensile strain of the steel tube reaches 10000 $\mu\varepsilon$, the computation stops.

3.3. Comparisons between Calculated and Tested Results. Eccentric load calculation program PYZTF was developed in accordance with the theories above. N versus u_m relationship curves were yielded by inputting the data to the program. Comparison between the calculated results and tested data is drawn in Figure 8, and it is shown that they are consistent well with each other.

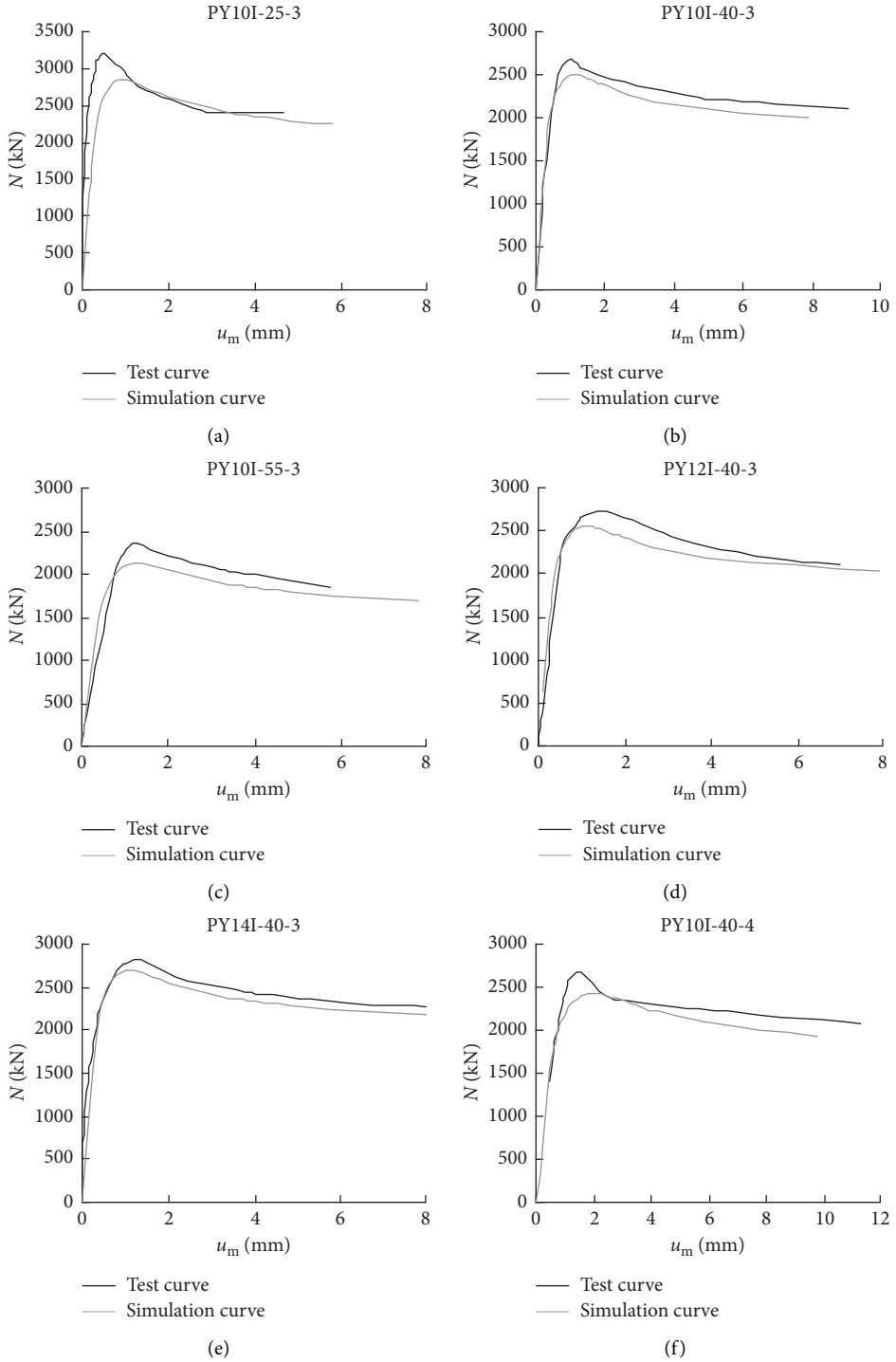

Figure 8: Continued.

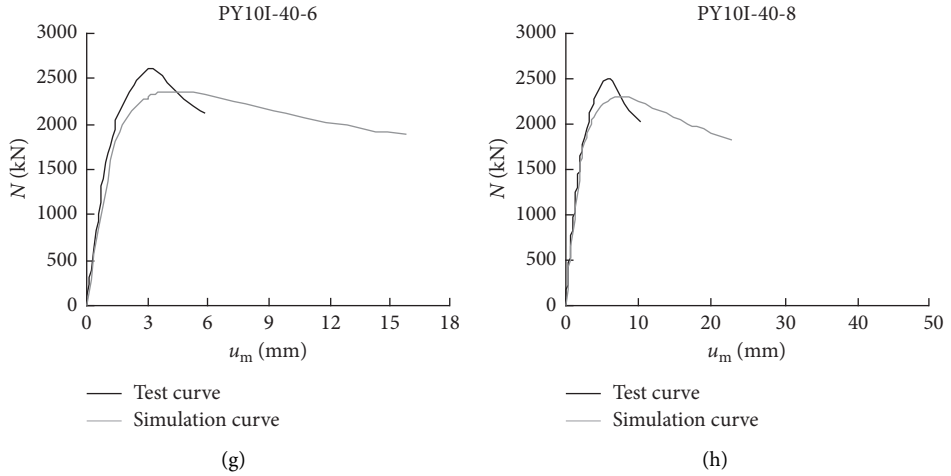

Figure 8: Comparisons between the calculated and tested results.

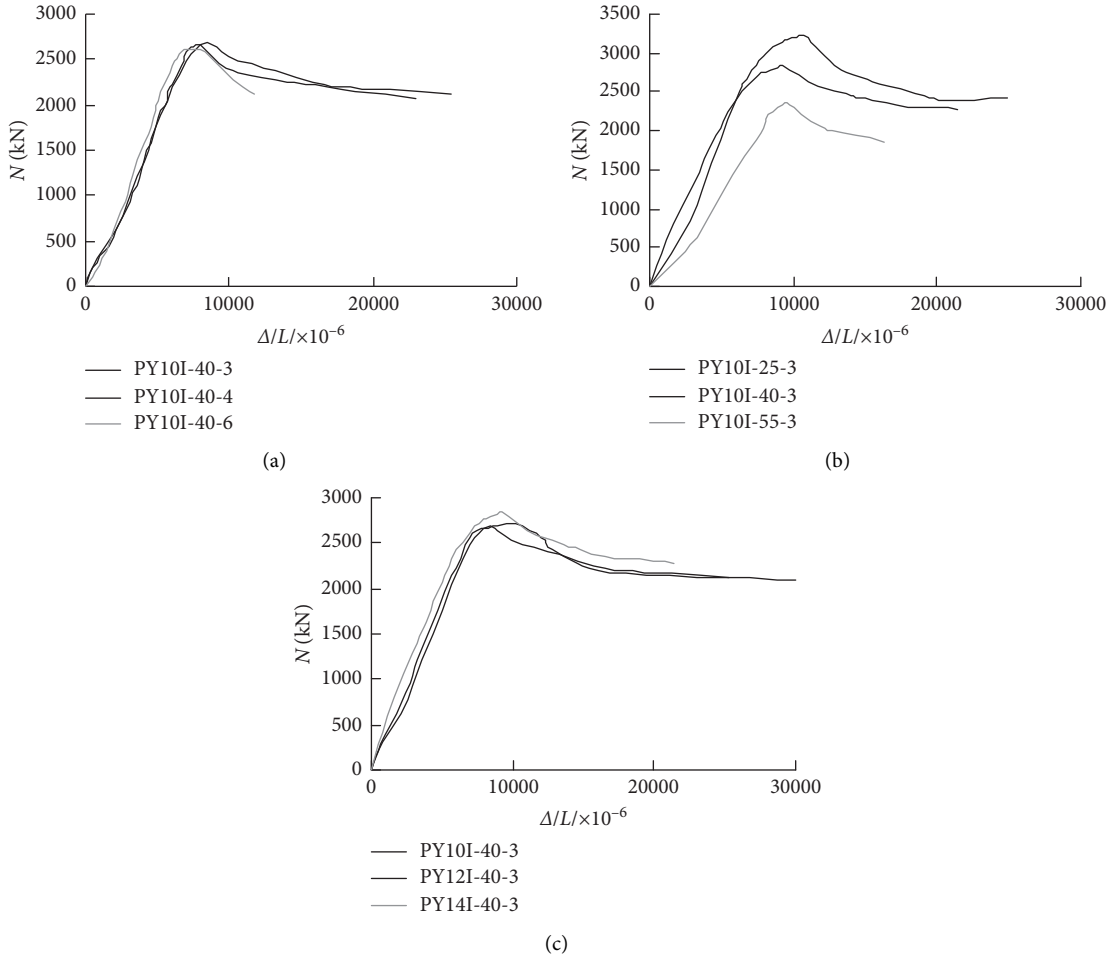

Figure 9: Influence of parameters on N-Δ: (a) slenderness ratios, (b) eccentricities, and (c) steel section ratios.

3.4. Simplified Calculation Method of Ultimate Bearing Capacity. Though the ultimate bearing capacity can be calculated accurately by program PYZTF, it is not adequate for practical application owing to the relatively complicated procedure. Thus, a simplified method is required to calculate the ultimate bearing capacity.

First, parameters including initial eccentricity e_o were inputted to the program. Next, the ultimate force N_u and

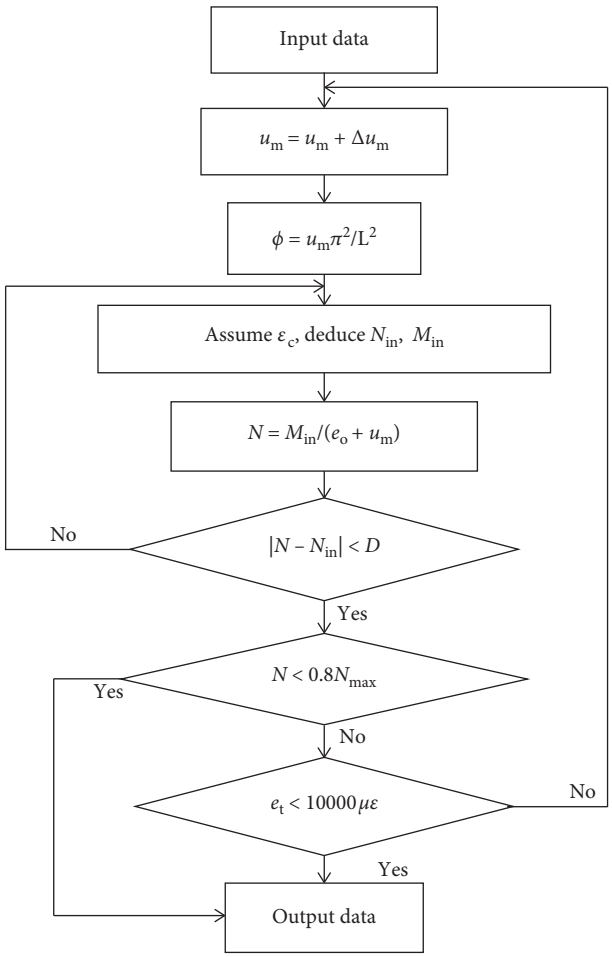

Figure 10: The algorithm of calculation.

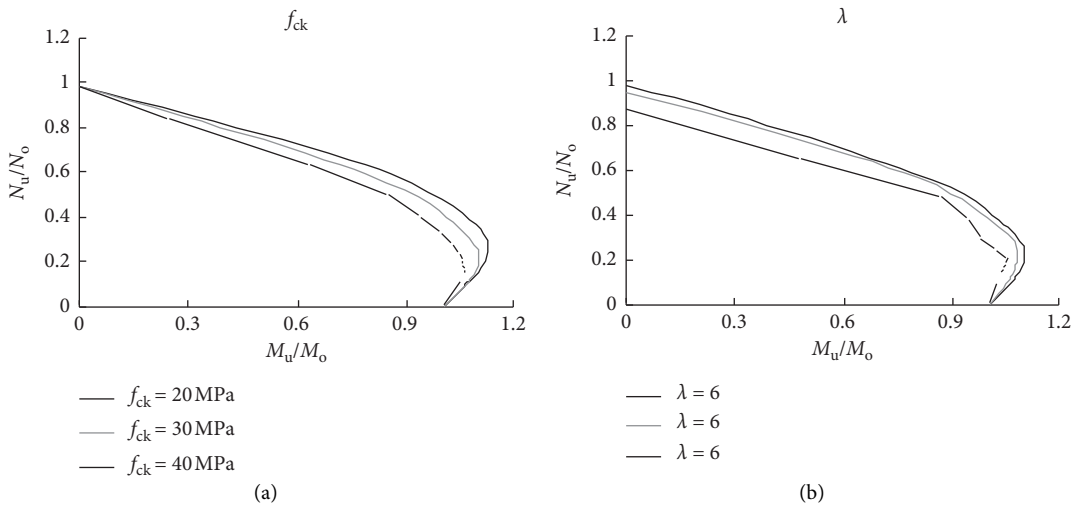

Figure 11: Continued.

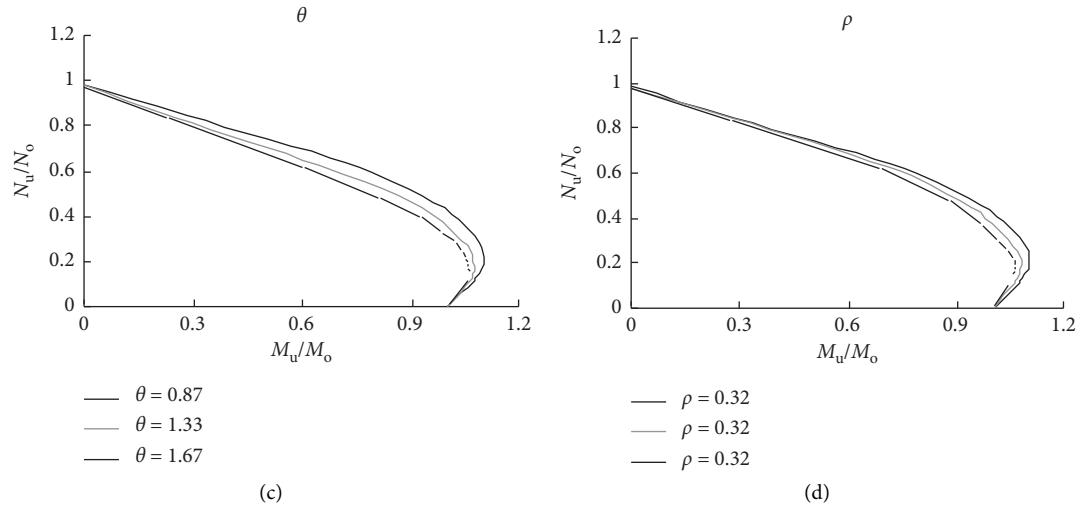

Figure 11: Influence of parameters on $N_u/N_o - N_u/N_o$.

corresponding moment M_u could be obtained. In the coordinate system, N_u/N_o was set as the perpendicular coordinate axis and N_u/N_o as horizontal coordinate axis. Thus, coordinate point $(N_u/N_o, N_u/N_o)$ was found. By changing E_o gradually, curves of N_u/N_o versus N_u/N_o can be plotted with different parameters. For instance, parameters of specimen in Figure 11 are $\lambda = 6$, $f_{ck} = 30$ MPa, $\theta = 0.87$, and $\rho = 0.32$.

Simplified curves of N_u/N_o versus N_u/N_o can be separated into two lines AB and BC (Figure 12) according to [3]. The accuracy of columns under small eccentricity and the safety under big eccentricity of both results were considered. Dashed line in Figure 12 represents a typical N_u/N_o versus N_u/N_o relationship curve.

The equation for ultimate bearing capacity was proposed using the regression method while considering the effect of reduction factor due to the slenderness of column (φ) on ultimate bearing capacity:

$$\begin{cases} N_u = \dfrac{\varphi}{(1/N_0) + (\eta e_0/M_0)}, & \dfrac{N}{N_0} \geq \varphi - a, \\ N_u = \dfrac{M_0}{\eta e_0}, & \dfrac{N}{N_0} < \varphi - a, \end{cases} \tag{3}$$

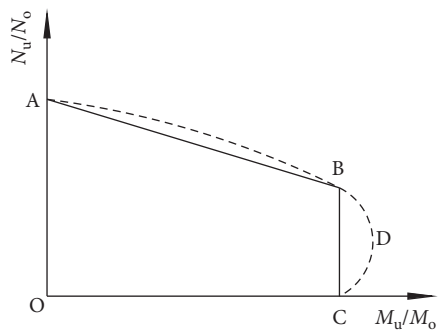

Figure 12: The simplified curve for N_u/N_o–N_u/N_o.

where $\eta = (1 + 0.003\lambda^{1.67})(2e_0/B) - 0.003\lambda^{1.5}$, $a = [0.375 + 0.746\exp(-1.394/0.566\theta + \rho)] \cdot \varphi$.

According to Zhao and Wang [3], the ultimate bearing capacity of the stub column under axial compression is given by $N_0 = (1 + \gamma\theta + \rho)A_c f_{ck}$,.$\gamma = 1.166 + 0.912\exp^{(-3.57\theta)}$ as

$$\varphi = \begin{cases} 1 - 0.65\overline{\lambda}, & \overline{\lambda} \leq 0.215, \\ 2\overline{\lambda}^2\left[\left(0.965 + 0.3\overline{\lambda} + \overline{\lambda}^2\right) - \sqrt{\left(0.965 + 0.3\overline{\lambda} + \overline{\lambda}^2\right)^2 - 4\overline{\lambda}^2}\right], & \overline{\lambda} > 0.215, \end{cases} \tag{4}$$

where $\overline{\lambda}$ denotes the relative slenderness ratio, $\overline{\lambda} = L/\pi\sqrt{(A_c f_c + 1.2A_t f_{ty} + A_s f_{sy})/(0.6E_c I_c + E_t I_t + E_s I_s)}$.

According to Mossahebiet al. [9], the ultimate moment of the column under pure bending is given by $M_0 = 0.5\xi \cdot B \cdot N_0$, where ξ denotes the plastic development

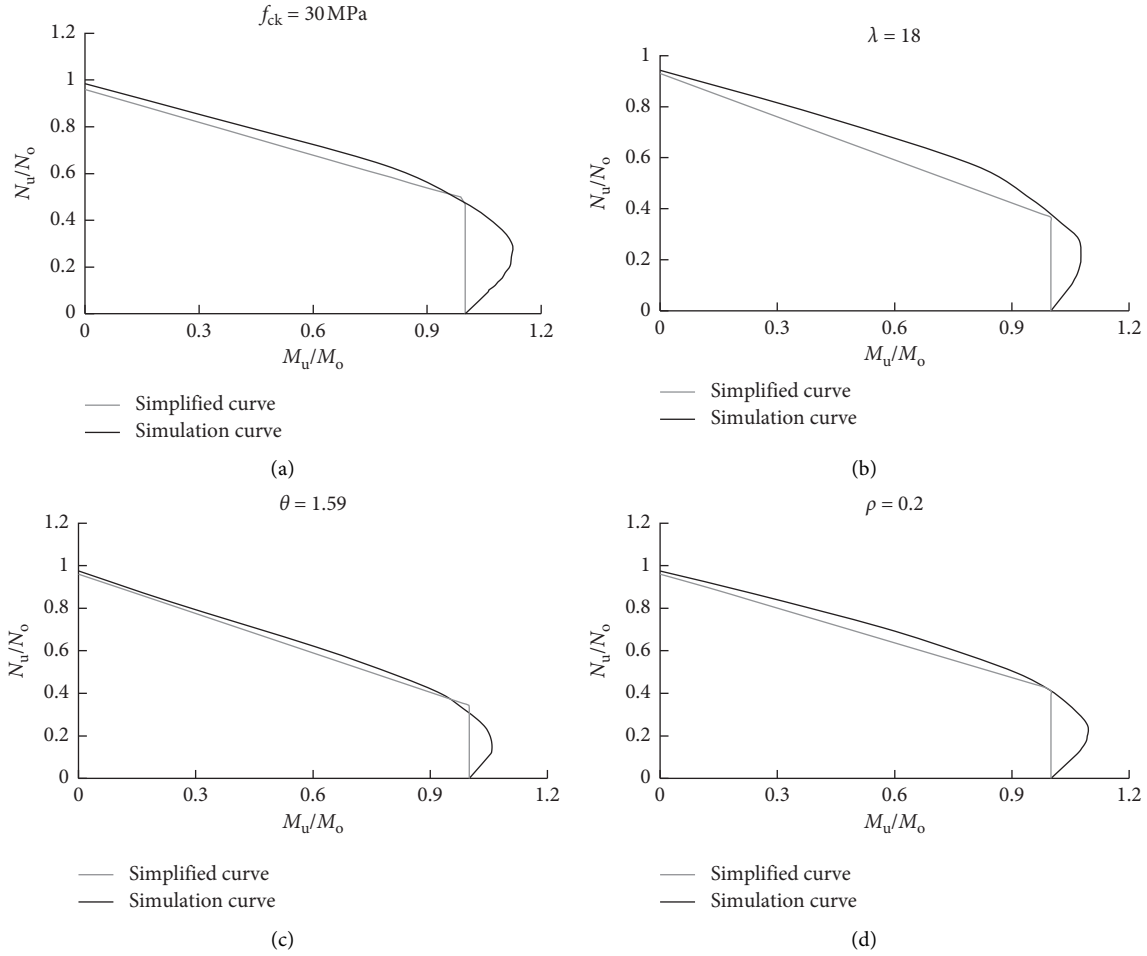

Figure 13: Comparisons between the fiber theoretical model and the simplified curves of $N_u/N_o - M_u/M_o$.

coefficient, $\xi = (0.134 + 0.613\sqrt{\theta} - 0.158\theta) \cdot (0.81 + 0.06\rho)(I/I_s)^{-0.048}$.

I, I_c, I_t, and I_s denote the second moment of whole area, concrete, steel tube, and steel cross section, respectively, and E_c, E_t, and E_s denote elastic modulus of concrete, steel tube, and steel, respectively.

The formula can be applied once the following condition is met: $\lambda = 3$–30, $f_{ck} = 20$–60 MPa, $f_{ty} = 235$–450 MPa, $f_{sy} = 235$–450 MPa, $\theta = 0$–3, and $\rho = 0$-1.

The tested parameters were inputted into program PYZTF and equation (3), respectively. The results are listed in Table 1. When the average value of N_{ue}/N_{us} is 1.083, the mean square deviation is up to 0.020. When the average value of N_{ue}/N_{uc} is 1.093, the mean square deviation reaches 0.019. Experimental data appear to be higher than the corresponding theoretical value. It was estimated that friction was produced by groove hinge and spherical hinges under high axial compression. Thus, the constraint to both ends of specimens was provided, and freedom of the specimen was restrained. Furthermore, the increased end decreased the geometrical length of columns, causing further increase in the bearing capacity.

Data of specimens ($\lambda = 6$, $f_{ck} = 30$ MPa, $\theta = 0.87$, and $\rho = 0.32$) were input into the simplified model and program PYZTF. Simplified N-M integration curves were verified by the fiber theoretical model (Figure 13). It can be found that, generally, good agreement is obtained between the fiber theoretical model and simplified model. Simplified model is acceptable to predict the bearing capacity of STRSC under eccentric load.

4. Conclusions

(1) Eccentricity significantly affects the bearing capacity; big eccentricity should be avoided in practical engineering.

(2) Slenderness ratio slightly affects capacity in tested parameters, i.e., slenderness ranges from 3 to 8. It is due to the high bending stiffness of STSRC.

(3) Bearing capacity with adequate precision can be calculated by equation (3) without any repeated computation. This equation can express mechanical properties of columns under the eccentricity.

Nomenclature

A_c, A_t, and A_s: Area of concrete, steel tube, and steel cross section, respectively

I, I_c, I_t, and I_s:	Second moment of whole area of concrete, steel tube, and steel cross section, respectively
E_c, E_t, and E_c:	Elastic modulus of concrete, steel tube, and steel, respectively
λ:	Slender ratio of column, $\lambda = L/B$
Δ:	Axial deformation
L:	Length of the specimen
B:	Side length diameter of the square steel tube
t;:	Thickness of the steel tube
e:	Eccentricity
e_0:	Initial eccentricity
ρ:	Steel reinforced index, λ
θ:	Confinement index, λ
ε:	Strain
f_{sy}:	Uniaxial yield stress of the steel section
f_{ty}:	Uniaxial yield stress of the steel tube
f_{ck}:	Compression strength of the unconfined concrete column
N:	Applied load
N_0:	Ultimate bearing capacity of the stub column under axial compression
N_u:	Ultimate bearing capacity of the column
M_0:	Ultimate moment of the column under pure bending
M_u:	Ultimate moment of the column under bending
φ:	Reduction factor due to the slenderness of the column.

Data Availability

The data used to support the findings of this study are available from the corresponding author upon request.

Conflicts of Interest

The authors declare that they have no conflicts of interest.

References

[1] D. Z. Zhao, Q. X. Wang, and P. Guan, "Calculation of bearing capacity of eccentrically loaded circular steel columns filled with steel-reinforced high-strength concrete," *Journal of China Harbor Engineering*, vol. 123, no. 2, pp. 26–28, 2013.

[2] Q. Wang, M. Zhu, and X. Feng, "Experimental study on axially loaded square steel tubes filled with steel reinforced self consolidating high strength concrete," *Journal of Building Structures*, vol. 26, no. 4, pp. 27–31, 2005.

[3] T. F. Zhao and L. G. Wang, "Calculation on compression-bending of square tube filled with steel-reinforced high-strength concrete," *Journal of Engineering Mechanics*, vol. 25, no. 10, pp. 122–125, 2017, in Chinese.

[4] T. F. Zhao and L. G. Wang, "Analysis on axially-loaded short columns of square steel tube filled with steel-reinforced concrete," *Journal of Industrial Construction*, vol. 35, no. 2, pp. 54–57, 2017, in Chinese.

[5] T. F. Zhao and L. G. Wang, "Capacity analysis on pure bending of square steel tube filled with steel-reinforced high strength concrete," *Journal of Northeastern University*, vol. 28, no. 9, pp. 1338–1341, 2017, in Chinese.

[6] V. I. Patel, Q. Q. Liang, and M. N. S. Hadi, "Biaxially loaded high-strength concrete-filled steel tubular slender beam-columns, part II: parametric study," *Journal of Constructional Steel Research*, vol. 110, no. 75, pp. 200–207, 2015.

[7] J. K. Jung and R. T. Mahmoud, "Experimental and numerical evaluation of direct tension test for cylindrical concrete specimens," *Advances in Civil Engineering*, vol. 2016, 8 pages, 2014.

[8] L.-H. Han, X.-L. Zhao, and Z. Tao, "Tests and mechanics model for concrete-filled SHS stub columns, columns and beam-columns," *Steel and Composite Structures*, vol. 1, no. 1, pp. 51–74, 2001.

[9] Y.-F. Yang and L.-H. Han, "Behaviour of concrete filled steel tubular (CFST) stub columns under eccentric partial compression," *Thin-Walled Structures*, vol. 49, no. 2, pp. 379–395, 2011.

[10] N. Mossahebi, A. Yakel, and A. Azizinamini, "Experimental investigation of a bridge girder made of steel tube filled with concrete," *Journal of Constructional Steel Research*, vol. 61, no. 3, pp. 371–386, 2005.

[11] X. Zhou, B. Yan, and J. Liu, "Behavior of square tubed steel reinforced-concrete (SRC) columns under eccentric compression," *Thin-Walled Structures*, vol. 91, pp. 129–138, 2015.

[12] X. Wang, J. Liu, and X. Zhou, "Behaviour and design method of short square tubed-steel-reinforced-concrete columns under eccentric loading," *Journal of Constructional Steel Research*, vol. 116, pp. 193–203, 2016.

[13] Y. Yang, Y. Wang, F. Fu, and J. Liu, "Static behavior of T-shaped concrete-filled steel tubular columns subjected to concentric and eccentric compressive loads," *Thin-Walled Structures*, vol. 95, pp. 374–388, 2015.

[14] N. Liu, "Experimental behaviour of cold-formed steel welded tube filled with concrete made of crushed crystallized slag subjected to eccentric load," *Thin-Walled Structures*, vol. 80, no. 1, pp. 159–166, 2014.

[15] C. Ju, J. Wang, and L. Wei, "Experimental behaviour of reinforced concrete-filled steel tubes under eccentric tension," *Journal of Constructional Steel Research*, vol. 136, pp. 91–100, 2017.

[16] J. M. Portolés, M. L. Romero, J. L. Bonet, and F. C. Filippou, "Experimental study of high strength concrete-filled circular tubular columns under eccentric loading," *Journal of Constructional Steel Research*, vol. 67, no. 4, pp. 623–633, 2011.

[17] G. Filippou, F. Giussani, G. Rosati, and F. Mola, "Response of self-compacting concrete filled tubes under eccentric compression," *Journal of Constructional Steel Research*, vol. 67, no. 5, pp. 904–916, 2011.

[18] S. Mola and C. Dundar, "Experimental study on steel tubular columns in-filled with plain and steel fiber reinforced concrete," *Thin-Walled Structures*, vol. 48, no. 6, pp. 414–422, 2010.

[19] H.-S. Jung, B.-I. Bae, H.-K. Choi, J.-H. Chung, C.-S. Chung, and Y.-C. Choi, "Experimental and numerical study on the compression behavior of square concrete-filled steel tube stub columns with steel fiber-reinforced high-strength concrete," *International Journal of Polymer Science*, vol. 2018, 13 pages, 2018.

[20] GB 50017, *Standard for Design of Steel Structures*, Ministry of Housing and Urban-Rural Development, Beijing, China, 2017, in Chinese.